

Manipulating Deposition Behavior by Polymer Hydrogel Electrolyte Enables Dendrite-Free Zinc Anode for Zinc-Ion Hybrid Capacitors


Chengzhe Liu, Fengjiao Guo, Qi Yang, Hongyu Mi,* Chenchen Ji, Nianjun Yang,* and Jieshan Qiu*

Rechargeable aqueous zinc-ion hybrid capacitors (ZHCs) have aroused unprecedented attention because of their high safety, cost effectiveness, and environmental compatibility. However, the intractable issues of dendrite growth and side reactions at the electrode–electrolyte interface deteriorate durability and reversibility of Zn anodes, deeply encumbering the large-scale application of ZHCs. Concerning these obstacles, a negatively charged carboxylated chitosan-intensified hydrogel electrolyte (CGPPHE) with cross-linked networks is reported to stabilize Zn anodes. Beyond possessing good mechanical characteristics, the CGPPHE with polar groups can reduce the desolvation energy barrier of hydrated Zn^{2+} , constrain the 2D Zn^{2+} diffusion, and uniformize electric field and Zn^{2+} flux distributions, assuring dendrite-free Zn deposition with high plating–stripping efficiency. Concurrently, the hydrophilic CGPPHE alleviates harmful hydrogen evolution and corrosion by abating water activity. Accordingly, Zn|CGPPHE|Zn and Zn|CGPPHE|Cu cells exhibit an extended life exceeding 350 h (1600 mAh cm^{-2} cumulative capacity under 20 mA cm^{-2}) and a high average coulombic efficiency of 98.2%, respectively. The resultant flexible ZHCs with CGPPHE and template-regulated carbon cathode present perfect properties in capacity retention (97.7% over 10 000 cycles), energy density (91.8 Wh kg^{-1}), and good mechanical adaptability. This study provides insight into developing novel hydrogel electrolytes toward highly rechargeable and stable ZHCs.

1. Introduction

Aqueous Zn-ion hybrid capacitors (ZHCs) are regarded as sustainable supplements to supercapacitors because of their high theoretical capacity, excellent power density, and relatively high energy density.^[1–4] The rechargeable function of ZHCs relies heavily on the plating–stripping process on the Zn anode and the adsorption–desorption process on the carbon cathode.^[3] Nevertheless, the reversible cycling of Zn anodes is troubled by the problems of notorious Zn dendrite growth and intricate side reactions, which impedes the performance progress and wide-range application of Zn-based energy storage systems.^[5–7] The generation of Zn dendrites stems from the unevenly distributed electric field and concentration polarization, which triggers the rapid attenuation of the coulombic efficiency (CE) and the internal short circuit of devices.^[8,9] More problematically, baneful interfacial side reactions, including hydrogen evolution reaction (HER) and corrosion caused by high-water-activity aqueous solution, exacerbate the dendrite issue.^[10,11] At present,

C. Liu, F. Guo, H. Mi, C. Ji
State Key Laboratory of Chemistry and Utilization of Carbon
Based Energy Resources
School of Chemical Engineering and Technology
Xinjiang University
Urumqi 830017, P. R. China
E-mail: mmihongyu@xju.edu.cn

 The ORCID identification number(s) for the author(s) of this article can be found under <https://doi.org/10.1002/smt.202201398>.

© 2022 The Authors. Small Methods published by Wiley-VCH GmbH. This is an open access article under the terms of the Creative Commons Attribution-NonCommercial License, which permits use, distribution and reproduction in any medium, provided the original work is properly cited and is not used for commercial purposes.

DOI: 10.1002/smt.202201398

Q. Yang, J. Qiu
State Key Laboratory of Chemical Resource Engineering
College of Chemical Engineering
Beijing University of Chemical Technology
Beijing 100029, P. R. China
E-mail: qiujs@mail.buct.edu.cn

N. Yang
Institute of Materials Engineering
University of Siegen
57076 Siegen, Germany
E-mail: nianjun.yang@uni-siegen.de

modifications of the anode and the electrolyte are emerging as good options to circumvent the issues of Zn anodes for efficiency improvement.^[12–14] However, the current electrolyte optimization primarily focuses on additive selection, which may be powerless to deal with the liquid leakage and mechanical tolerance problems of aqueous devices with liquid electrolyte (LE).

To compromise the above challenges, “beyond aqueous” electrolytes have extensively been considered recently, among which highly safe polymeric hydrogel electrolytes are particularly launched due to their marked merits over the ordinary LE.^[15] Through the molecular-level adjustment of the polymeric matrix, the designed polymer-based hydrogel electrolytes with special functional groups are capable of visibly achieving intelligent functions.^[16] For instance, some zincophilic and hydrophilic groups of the polymeric matrix in such electrolytes are prone to guiding Zn²⁺ transport and depressing the water activity, thus mitigating the dendrite and side reaction issues to a certain extent.^[17,18] Despite these apparent advantages, two underlying confinements should be well liberated to gain more reversible and stable Zn anodes in polymer hydrogel electrolytes. One is that Zn²⁺ adsorbed on the anode tends to migrate horizontally along the surface (defined as 2D diffusion) to search for energetically favorable tip sites and reduce to Zn⁰ on tips, which intensifies the nonuniform electric field and hence leads to dendritic growth.^[19,20] The other is that the desolvation process of hydrated Zn²⁺ in aqueous electrolytes inevitably consumes a huge amount of energy due to the strong coulombic interaction between Zn²⁺ and H₂O solvation sheath.^[21,22] The large desolvation penalty is highly likely to provoke HER and hinder Zn deposition kinetics.^[23] Recent research has proved that some polar groups carried by polymer chains, especially negatively charged groups (e.g., sulfonate, phosphate, and carboxyl groups), preferentially interact with Zn²⁺, realizing the dual effects of changing the solvation structure to reduce the desolvation barrier of hydrated Zn²⁺ and redistributing the ion flux to constrain 2D diffusion.^[17,24–28] Additionally, favorable mechanical properties of such electrolytes are requisite, which guarantees the firm interface contact with the electrode in daily activities to stabilize Zn anodes for flexible and high-performance Zn-based devices.^[29] Nevertheless, the polymer hydrogel electrolytes with the above comprehensive features remain scarce, and thus deeply understanding their impact on electrochemical properties is immensely important for further boosting the function of hydrogel electrolytes.

Considering that negatively charged carboxylated chitosan (CCS) features multiple merits, such as rich resources, environmental benignity, macromolecule structure, and sufficient hydrophilic/polar groups, herein we propose a CCS-enhanced hydrogel electrolyte (CGPPHE) with multiple cross-linked networks to minimize the facing issues of Zn electrodes and achieve efficient and flexible ZHCs. The innovative CGPPHE consists of carboxylated chitosan-*graft*-polyacrylamide (CCS-*g*-PAM) and polyvinyl alcohol (PVA) permeated with zinc trifluoromethanesulfonate (Zn(OTf)₂) aqueous solution, harvesting satisfactory mechanical characteristics and ionic conductivity. Based on electrochemical tests, in situ microscopic observation, and density functional theory (DFT) calculations, we have proved that the prepared CGPPHE has diverse functions, namely, quickening the ion transport, reducing the

desolvation energy barrier of hydrated Zn²⁺, restricting the 2D ion diffusion at Zn electrode surface, and immobilizing water molecules, which benefits from the strongly polar and hydrophilic carboxyl groups of CCS assisted by amide groups of PAM. Therefore, CGPPHE displays the excellent ability to restrain dendrite generation, corrosion, and HER as compared to its counterparts (PPHE and PHE), where PPHE and PHE are hydrogel electrolytes with polymeric matrices of PAM/PVA and PAM, respectively. These properties enable the stable cycling of more than 350 h at 1 mA cm⁻² for the Zn|CGPPHE|Zn cell and the high average CE of 98.2% after 700 cycles at 4 mA cm⁻² for the Zn|CGPPHE|Cu cell. Moreover, a respectable cumulative capacity of 1600 mAh cm⁻² is delivered at 20 mA cm⁻². Due to the above advantages, the flexible ZHC made of CGPPHE, template-assisted porous carbon (TPC) cathode and Zn anode has long-term cycling stability, outstanding energy and power densities (91.8 Wh kg⁻¹ and 15 685.7 W kg⁻¹), and high working reliability under bending deformation.

2. Results and Discussion

PAM and CCS would be decorated by the grafting or cross-linking reaction, and PVA can be readily bound to many molecules (PAM, CCS, etc.) through hydrogen-bonding interaction.^[30–33] Inspired by these features, herein the molecular engineering based on these components is applied in the design of functional hydrogels. As briefly schematized in **Figure 1a**, we first prepared a homogeneous colloid embracing CCS, PVA, acrylamide (AM) monomer, ammonium persulfate initiator, and *N,N'*-methylenebisacrylamide (MBAA) cross-linker in deionized water. The subsequent thermal polymerization gave rise to the grafting of the formed PAM chains on the CCS backbone and the cross-linking between PAM chains, producing a chemically cross-linked CCS-*g*-PAM hydrogel with rich functional species.^[31] Meanwhile, the CCS-*g*-PAM backbone was bound to the PVA chain via extensive hydrogen bonds and mechanical entanglement to build a network-like hydrogel matrix of CCS-*g*-PAM/PVA (CGPPH).^[32,33] Digital images visually confirm the successful transition from the precursor solution to a transparent solid-like hydrogel (CGPPH) after heating (**Figure 1b**). Next, a highly robust hydrogel electrolyte with multiple networks (CGPPHE) was received by impregnation of CGPPH in 1 M Zn(OTf)₂ aqueous solution. **Figure 1c** illustrates the chemical structure of CGPPHE with sufficient covalent and hydrogen bonds. To confirm the presence of functional groups in CGPPH, Fourier-transform infrared (FTIR) spectrum analysis was carried out (**Figure 1d**). The broad absorption peak appeared at 3500–3074 cm⁻¹ reflects the stretching vibrations of N–H and O–H groups raised from PAM, PVA, and CCS components.^[34] The three peaks at around 2926, 1644, and 1407 cm⁻¹ are the stretching vibrations of C–H (2925 cm⁻¹ for PAM and 2906 cm⁻¹ for PVA), C=O (1647 cm⁻¹ for PAM and 1641 cm⁻¹ for CCS), and O=C–O (1400 cm⁻¹ for CCS), respectively.^[31,34–36] As for the signal peak at ≈1030 cm⁻¹, it corresponds to the C–OH stretching (1025 cm⁻¹ for CCS and 1084 cm⁻¹ for PVA).^[37] Noticeably, the position and intensity of the above peaks in CGPPH slightly deviate from those in pristine PAM, PVA, and CCS, which may be ascribed to the chemical and physical

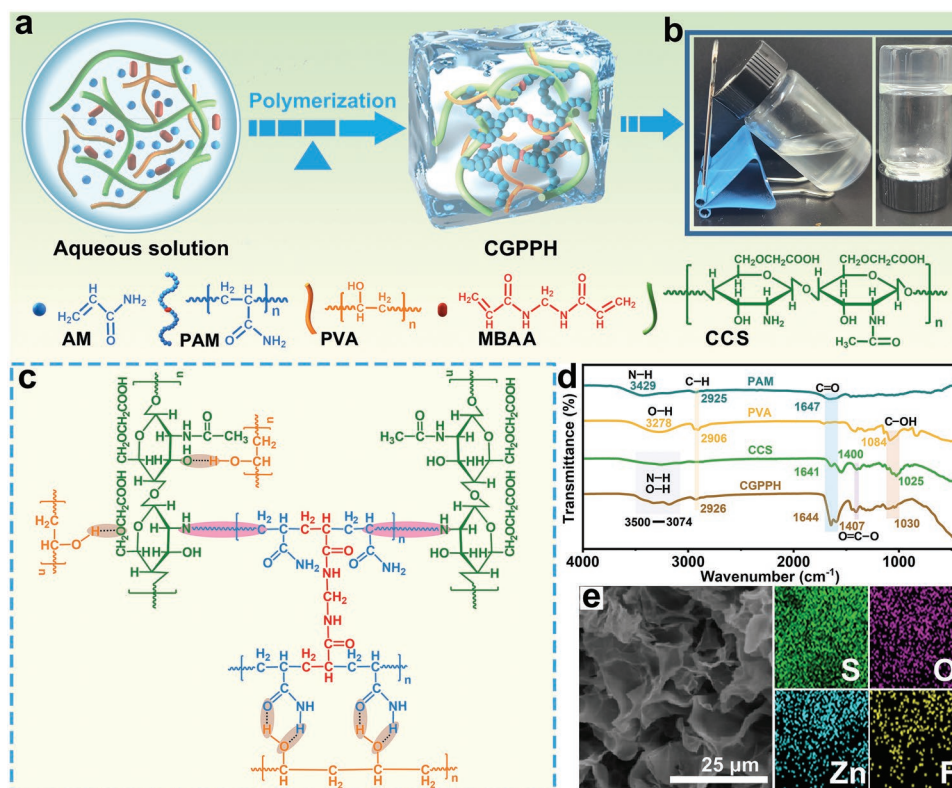


Figure 1. Synthesis and characterization of CGPPH. a) Schematic of CGPPH synthesis. b) Digital photographs showing the successful completion of CGPPH. c) The chemical structure of CGPPH. d) FTIR spectra of PAM, PVA, CCS, and CGPPH. e) SEM image of the freeze-dried CGPPHE with corresponding EDS elemental mappings.

interactions between these constituents. FTIR results reveal the existence of hydrophilic carboxyl, amide, and hydroxyl groups in CGPPH, which helps to immobilize water molecules through hydrogen-bonding interaction, thereby weakening the activity of water and mitigating water-induced corrosion and HER.^[15,25,38,39] The scanning electron microscopy (SEM) image clearly shows a macropore-interconnected framework, and the corresponding energy dispersive spectroscopy (EDS) mappings confirm the good distribution of S, O, Zn, F, and C elements in the freeze-dried CGPPHE (Figure 1e; Figure S1, Supporting Information). It is conjectured that such a porous CGPPHE has intrinsically high ionic conductivity.

Figure 2a–d confirms superior mechanical properties of CGPPHE to its counterparts (PHE and PPHE). As depicted in Figure 2a, the tensile stress of CGPPHE under 473.7% strain is 69.6 kPa, while the corresponding values of PHE and PPHE are only 3.6 kPa under 131.4% strain and 10.7 kPa under 284.9% strain. CGPPHE still holds up well when stretched to 400% strain, signifying its excellent ductility (the insets in Figure 2a). Similarly, CGPPHE has good compressibility, with a compressive stress of 151.2 kPa at 60% strain, in comparison with PHE (9.5 kPa) and PPHE (11.1 kPa) (Figure 2b and its inset). The significantly improved properties of CGPPHE correlate closely to strong chemical/physical interactions and massive hydrogen bonds that exist in cross-linked networks. Specifically, when CCS is integrated into the polymer backbone, it can interact with PAM by covalent bonds, and the generated CCS-g-PAM

dynamically interacts with PVA by hydrogen bonds and physical entanglement, jointly contributing to mechanical properties of the synthesized CGPPHE.^[31,33,40] Figure 2c presents the cyclic tensile curves under different strains (100–400%). The loading–unloading curves with pronounced hysteresis loops verify the good resilience and excellent fatigue resistance of CGPPHE.^[41] The compression–recovery curves show slight hysteresis loops with restorable compressive strain in 2–5 cycles except for the initial cycle, which reflects the good elasticity and rapid recoverability of CGPPHE (Figure 2d and its inset). This can be further verified by the digital photographs before and after 5 cycles of compression (the inset in Figure 2d), and SEM images showing an unspoiled macropore-interconnected network after cyclic compression (Figure S2, Supporting Information). In addition, CGPPHE has a slight thickness change after being assembled into the device, further verifying its approving mechanical properties that benefit the stable operation of this hydrogel electrolyte in devices (Figure S3, Supporting Information).

Apart from mechanical robustness, hydrogel electrolytes should be featured with strong adhesiveness to the electrode so as to avert the separation from the electrode. We chose electrode materials such as metal Zn, stainless steel, copper, and titanium sheets as substrates to assess this property of CGPPHE. As seen from digital photographs in Figure 2e, CGPPHE displays good adhesiveness to different metal substrates, which is attributed to the physical interactions between CGPPHE and substrates.^[42–44] The corresponding adhesive strengths

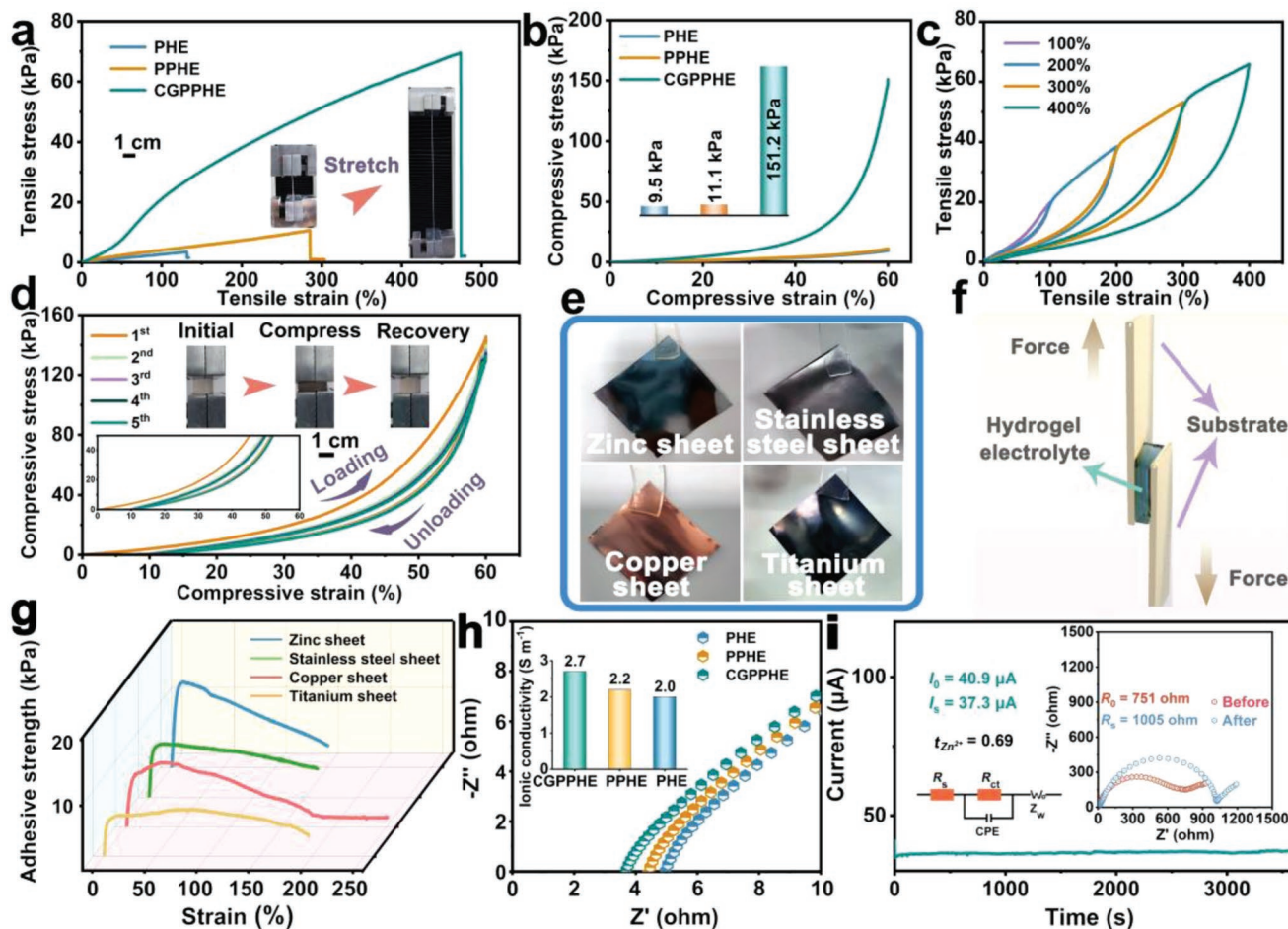


Figure 2. Mechanical properties and ion-transport ability of CGPPHE. a) Tensile stress–strain curves of PHE, PPHE, and CGPPHE (insets: digital photographs of CGPPHE during stretching). b) Compressive stress–strain curves of PHE, PPHE, and CGPPHE (inset: the corresponding compressive strength). c) Cyclic tensile curves of CGPPHE under different strains. d) Cyclic compressive curves of CGPPHE at 60% strain (insets: digital photographs of CGPPHE during compressing and enlarged curves near the zero point). e) Digital photographs showing good interface adhesion between CGPPHE and different substrates. f) Diagram of the adhesive test. g) Adhesive strength of CGPPHE on different substrates. h) Nyquist plots of PHE, PPHE, and CGPPHE (inset: the corresponding ionic conductivity). i) $I-t$ curve of the symmetric cell with Zn electrodes and CGPPHE at an applied voltage of 10 mV (inset: Nyquist plots before and after polarization).

of CGPPHE quantified by the lap shear test (Figure 2f) are 12.4 ± 1.4 , 8.7 ± 0.8 , 9.3 ± 0.6 , and 75 ± 0.8 kPa on Zn, stainless steel, copper, and titanium sheets, respectively (Figure 2g). It illustrates that the firm electrolyte–electrode interface can be established via the hydrogel electrolyte design, facilitating the full play of CGPPHE function for stabilizing Zn anodes.^[17,45]

The ionic conductivity (σ) and Zn^{2+} transference number ($t_{Zn^{2+}}$) of CGPPHE were measured to assess its ion-transport ability. It is known from electrochemical impedance spectroscopy (EIS) that CGPPHE has a larger σ value of $2.7 S m^{-1}$ than PPHE ($2.2 S m^{-1}$) and PHE ($2.0 S m^{-1}$) (Figure 2h and its inset), indicating the positive action of CCS in promoting the ionic transport. Moreover, the designed CGPPHE gains a higher $t_{Zn^{2+}}$ of 0.69 compared with PPHE (0.56) and LE (0.33) (Figure 2i). This indicates that the polar carboxyl and amide groups in CGPPHE can interact with cations to optimize Zn^{2+} transmission behavior,^[25,46,47] which is in favor of reducing the concentration polarization (the reduction of concentration difference

near to the Zn surface and further mitigating the dendritic growth.^[15,48]

In addition to mechanical damage, the dendrites, corrosion, and HER will also deteriorate the electrochemical stability and reversibility of Zn anodes, leading to performance degradation or even failure of energy storage systems. To survey the influence of different electrolytes on Zn deposition behavior, the real-time morphological evolution of Zn electrodes at 10 mA cm^{-2} was scrutinized by an optical microscope. Figure 3a (upper) shows that small protrusions emerge on Zn foil in LE after plating for 30 min, and massive dendrite-like aggregates are formed after 120 min due to the tip effect. Such a dendritic appearance can increase the surface area of the electrode to aggravate the surface-dependent side reactions, thereby reducing CE and shortening the cycle life of energy storage devices.^[49] After the use of PHE and PPHE, the scale of randomly distributed protrusions on Zn foil decreases to some extent (Figure S5, Supporting Information). In stark contrast,

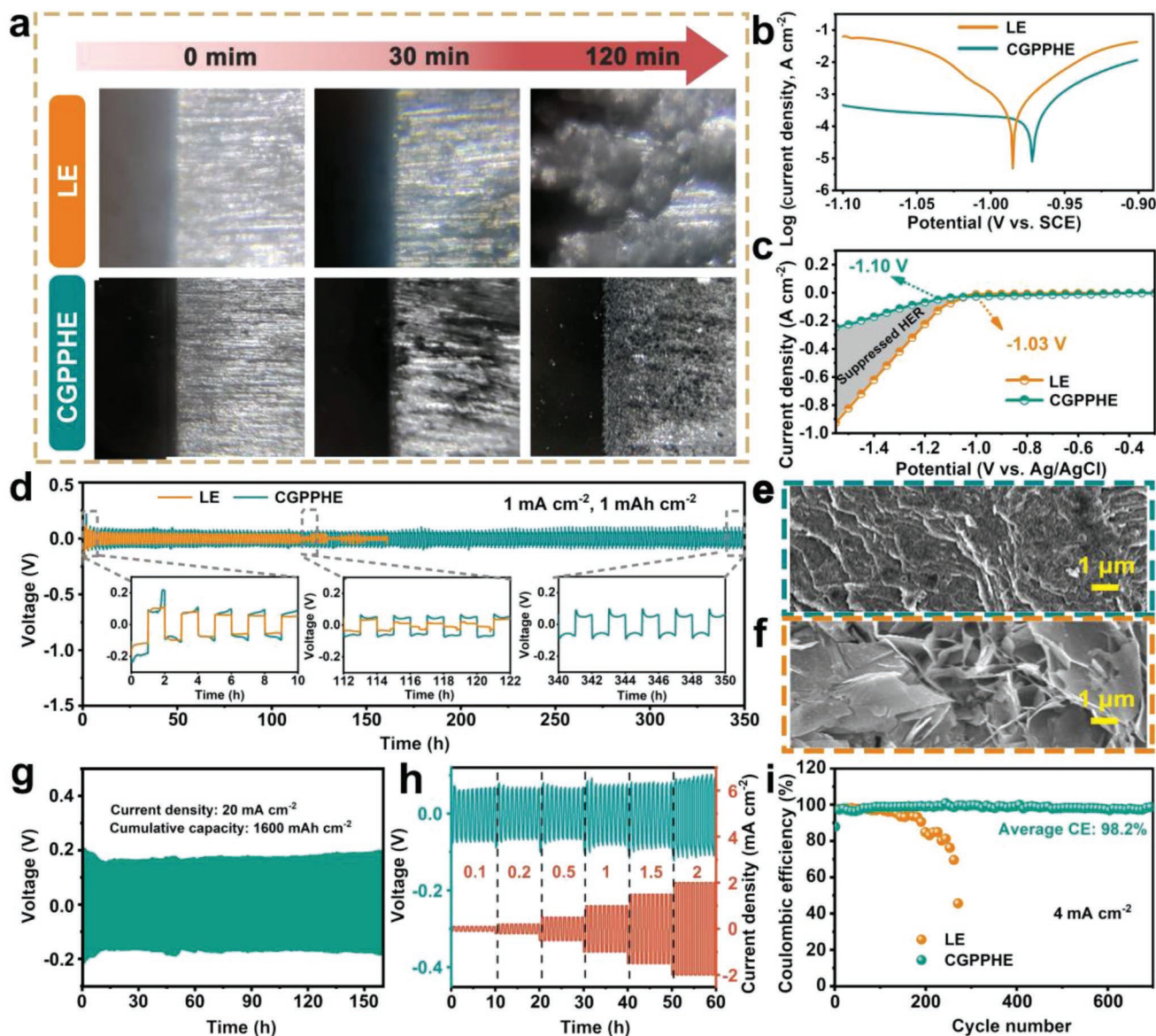


Figure 3. a) In situ optical microscopic images for Zn deposition in LE and CGPPHE. b) Linear polarization plots and c) LSV curves of Zn electrodes in LE and CGPPHE. d) Galvanostatic cycling stability of Zn|LE|Zn and Zn|CGPPHE|Zn cells at 1 mA cm^{-2} and 1 mAh cm^{-2} . SEM images of Zn electrodes after cycling in e) CGPPHE and f) LE. g) Galvanostatic cycling stability of Zn|CGPPHE|Zn cell at 20 mA cm^{-2} and 1 mAh cm^{-2} . h) Rate performance of the Zn|CGPPHE|Zn cell at different current densities. i) CE of Zn|LE|Cu and Zn|CGPPHE|Cu cells.

a relatively smooth surface without discernible dendrites can be observed on Zn during the whole plating in CGPPHE (Figure 3a). The contrastive results manifest the synergism of CCS and PAM in inhibiting dendrite growth, in which CCS has a more positive effect due to good regulation of its negatively charged groups on deposition behavior.^[50] As mentioned above, some hydrophilic groups in polymer chains can interact with water molecules through hydrogen bonds to efficiently subdue the water activity.^[15,25,38,39] It is thereby predicted that CGPPHE possessing abundant hydrophilic species may alleviate the corrosion and HER. To verify these predictions, the linear polarization tests of Zn electrodes in different electrolytes were first carried out. As shown in Figure 3b, the Zn electrode in CGPPHE

has a higher corrosion potential of -0.972 V than that in LE (-0.985 V). We conclude that the smaller corrosion tendency occur in CGPPHE, meaning good corrosion resistance of Zn in this electrolyte.^[7,51] From linear scanning voltammetry (LSV) curves (Figure 3c), it is found that the Zn electrode in CGPPHE compared to LE has a smaller current density, and the onset potential of HER increases by $\approx 70 \text{ mV}$, indicative of the suppressed HER in CGPPHE.^[11,27]

Profiting from the promotion effect of CGPPHE on confining dendrite growth and parasitic reactions, Zn anodes may possess good electrochemical durability, which is verified by galvanostatic cycling of the symmetric Zn|CGPPHE|Zn cell. As expected, the Zn|CGPPHE|Zn cell can be stably circulated for

more than 350 h at a current density of 1 mA cm⁻² with an area capacity of 1 mAh cm⁻² (Figure 3d). As a contrast, after stable cycling of ≈115 h, the Zn|LE|Zn cell exhibits a marked voltage fluctuation due to the dynamicity of the soft short-circuit,^[29] and subsequent rapid voltage decline with irrecoverability due to the device failure, manifesting poor cycling of Zn anode in LE.^[52] As for Zn|PHE|Zn and Zn|PPHE|Zn cells, their cycling performances are also inferior and remain at 165 and 193 h, respectively (Figure S6, Supporting Information). Comparatively, the distinctly prolonged life of the cell with CGPPHE is greatly associated with the introduced CCS with polar carboxyl groups. Figure 3e,f shows the surface morphology of Zn foils from the above cycled cells with CGPPHE and LE, respectively. Obviously, the large sheets are almost horizontally arranged on the Zn surface with specific orientation after cycling in CGPPHE for 350 h (Figure 3e). Whereas the surface of the cycled Zn foil in LE is quite rough, with vertically stacked dendrites (Figure 3f). The experimental results support that the designed CGPPHE can preferentially guide homogeneous deposition of Zn to mitigate the dendrite-induced life decline. Additionally, the X-ray diffraction analysis was conducted for identifying the composition of Zn foils cycled in LE and CGPPHE. The diffraction peaks representing Zn₁₂(CF₃SO₃)₉(OH)₁₅·xH₂O byproduct at 6.5°, 13°, and 19.6° are discernible on the Zn foil cycled in LE,^[53] but these peaks are not detected in CGPPHE (Figure S7, Supporting Information). It convincingly confirms that CGPPHE can reduce harmful corrosion and thus prolong the life of Zn anodes. The cycling performance of the Zn|CGPPHE|Zn cell even under 20 mA cm⁻² was probed as well. The excellent stability of 160 h with an ultrahigh cumulative capacity of 1600 mAh cm⁻² can be gained (Figure 3g). The cumulative capacity of the Zn|CGPPHE|Zn cell exceeds that of many recently reported cells with electrolyte regulation and other strategies (Table S1, Supporting Information). More encouragingly, the Zn|CGPPHE|Zn cell can work normally without erratic voltage response in a current range of 0.1 to 2 mA cm⁻² (Figure 3h), while the Zn|LE|Zn cell appears fluctuant voltage hysteresis as the current density increases (Figure S8, Supporting Information). In addition, the electrochemical reversibility of asymmetric cells with different electrolytes was studied. The average CE of the Zn|CGPPHE|Cu cell is recorded with a high value of 98.2% that stably maintains 700 cycles at 4 mA cm⁻² with a cut-off voltage of 0.7 V (Figure 3i). Besides, the significant contribution of CCS on the plating–stripping reversibility is clearly verified by the short-lived Zn|PPHE|Cu cell with 271 cycles at the same current density (Figure S9, Supporting Information). Regrettably, the CE of the Zn|LE|Cu cell dominantly decreases accompanied by serious fluctuation after 180 cycles due to dendrite growth and severe parasitic reactions (Figure 3i).^[54] Detailed galvanostatic charge–discharge (GCD) profiles of the Zn|CGPPHE|Cu cell show relatively stable voltage gaps from the beginning to the end, while the Zn|LE|Cu cell undergoes a consecutive voltage fluctuation (Figure S10, Supporting Information). Electrochemical results strongly verify the advantages of CGPPHE in the suppression of dendrites and side reactions, which favors a stable and reversible plating–stripping process to guarantee gratifying cyclability and energy output for the ZHCs with this hydrogel electrolyte.

In order to elucidate the desolvation kinetics in different electrolytes, the temperature-dependent EIS tests were carried out on symmetric Zn cells. During the plating process, the desolvation of hydrated Zn²⁺ ([Zn(H₂O)₆]²⁺) precedes the redox reaction between Zn²⁺ and Zn⁰ at the Zn electrode–electrolyte interface, and is usually considered as the rate-limiting step for Zn deposition, owing to the strong interaction between the solvated Zn²⁺ and the surrounding H₂O shell.^[55] Generally, the low desolvation energy barrier facilitates the desolvation, which can be described by the activation energy (*E*_a) from the Arrhenius equation

$$\frac{1}{R_{ct}} = A \exp\left(\frac{-E_a}{RT}\right) \quad (1)$$

where *R*_{ct}, *A*, *R*, and *T* are the charge-transfer resistance, frequency factor, gas constant, and temperature, respectively.^[22,23] Figure 4a and Figure S11 (Supporting Information) are Nyquist profiles of various cells at a temperature range of 10–60 °C. Obviously, the *R*_{ct} values of the Zn|CGPPHE|Zn cell at various temperatures are less than those of its counterparts, confirming the improved charge transfer capability in CGPPHE (Figure S12, Supporting Information).^[28] The *E*_a of the Zn|CGPPHE|Zn cell is estimated to be 32.8 kJ mol⁻¹, which is only 78.8% and 70.4% of the values for the Zn|PPHE|Zn cell (41.6 kJ mol⁻¹) and Zn|LE|Zn cell (46.6 kJ mol⁻¹) (Figure 4b). It means that compared with LE and amide-containing PPHE, hydrated Zn²⁺ in CGPPHE with carboxyl and amide groups has an easier desolvation process.^[24,56] Based on the above results, the improvement of desolvation kinetics in CGPPHE can be ascribed to the regulation of the solvation structure of Zn²⁺ by polar carboxyl and amide groups, where the former plays the prior role.^[27]

The effect of CGPPHE on the initial nucleation stage was further revealed by the nucleation overpotential (NOP) from the cyclic voltammetry (CV) test. As shown in CV profiles of Figure 4c, the potential difference between the crossover point (A) and the initial deposition point (B for CGPPHE and B' for LE) corresponds to the NOP, which is a key parameter to evaluate the nuclei radius from the following relationship^[5,57,58]

$$r_{crit} = 2 \frac{\gamma V_m}{F |\eta|} \quad (2)$$

where *r*_{crit}, *γ*, *V*_m, *F*, and *η* refer to the nuclei radius, surface energy of the Zn–electrolyte interface, molar volume of Zn, Faraday's constant, and NOP, respectively. Larger NOPs lead to smaller nuclei based on this relation. The NOP increases evidently from 65 mV in LE to 160 mV in CGPPHE, which indicates more fine-grained Zn deposits in CGPPHE.

Insights into the electrolyte ions' diffusion mode benefit the understanding of Zn nucleation/growth behavior, which is determined by chronoamperometric (CA) tests on symmetrical cells (Figure 4d). In LE, the current density progressively decreases within the duration of 200 s at a constant overpotential of -150 mV, which reflects the long and rampant 2D diffusion process of adsorbed Zn²⁺ along the electrode surface. The consecutive 2D diffusion gives rise to the accumulation of Zn²⁺ on the protuberances and results in rough deposition

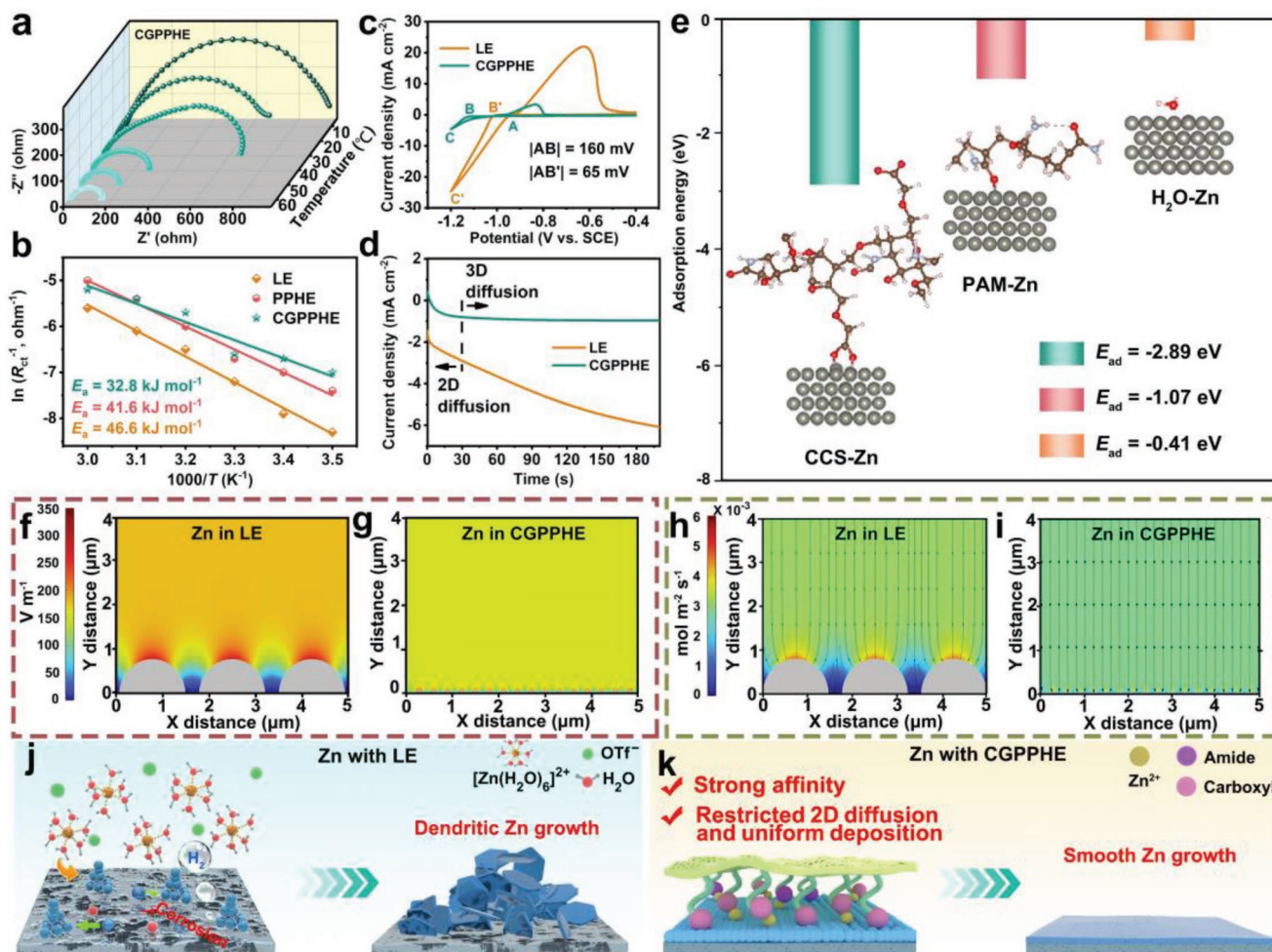


Figure 4. a) Nyquist plots of the Zn|CGPPHE|Zn cell at different temperatures. b) Arrhenius plots and derived desolvation activation energies for Zn|CGPPHE|Zn, Zn|PPHE|Zn, and Zn|LE|Zn cells. c) CV profiles for Zn nucleation in LE and CGPPHE. d) Chronoamperograms of Zn|LE|Zn and Zn|CGPPHE|Zn cells. e) DFT-calculated adsorption energies of CCS, PAM, and H₂O on Zn substrates. Electrical field distributions in f) LE and g) CGPPHE. Zn²⁺ flux distributions in h) LE and i) CGPPHE. Illustration of the Zn deposition process in j) LE and k) CGPPHE.

propagation based on the principle of minimizing the surface energy.^[59,60] By contrast, after the transient 2D diffusion with a decreased current density occurs in the early stage of deposition in CGPPHE (≈ 30 s), the stable 3D diffusion with a constant current density continues until the end. It means that the adsorbed Zn²⁺ on the electrode is locally reduced to Zn⁰ for uniform Zn deposition, which stems from the constrained 2D diffusion due to the strong affinity between the polar carboxyl and amide groups in CGPPHE and the Zn electrode.^[19] DFT calculations were conducted to theoretically analyze the CGPPHE–Zn electrode interaction. Figure 4e presents that the adsorption energy (-2.89 eV) of CCS on the Zn (002) plane is more negatively than that of PAM (-1.07 eV) and H₂O (-0.41 eV). It confirms that CGPPHE has a strong affinity with Zn atoms, and the carboxyl groups in CGPPHE are more easily associated with Zn electrode than amide groups. The adsorbed groups on metallic Zn may generate the electrostatic shielding to simultaneously restrict 2D diffusion of Zn²⁺ and prevent water molecules from contacting the Zn electrode, thus guiding dendrite-free deposition and reducing side reactions.^[27]

Finite element simulations were provided to elaborate the influence of different electrolytes in harmonizing Zn²⁺ flux and electric field distributions (Figure 4f–i). In virtue of the sustained 2D Zn²⁺ diffusion at the Zn–LE interface, large and sporadic protuberances emerge on the Zn electrode, resulting in the exaggerated electric field heterogeneity near protuberant tips (Figure 4f).^[61] The tip-aggregated electric field intensifies the Zn²⁺ aggregation near protuberances, making the worse homogeneity of the Zn²⁺ flux distribution and causing further growth of dendrites (Figure 4h).^[62] Compared with LE, CGPPHE ensures the fine-grained Zn nucleation and limited 2D Zn²⁺ diffusion, which contributes to the well-distributed electric field (Figure 4g). Such an electric field can homogenize Zn²⁺ flux to realize satisfactory Zn deposition (Figure 4i). Different Zn deposition behaviors in LE and CGPPHE are schematically illustrated in Figure 4j,k. The tip effect is the culprit for the dendritic Zn growth in traditional aqueous electrolytes. Sparse protuberances in LE induced by rampant 2D Zn²⁺ diffusion trigger the tip-aggregated electric field, causing the accumulation of Zn²⁺ around the tips to form dendrites. Worse,

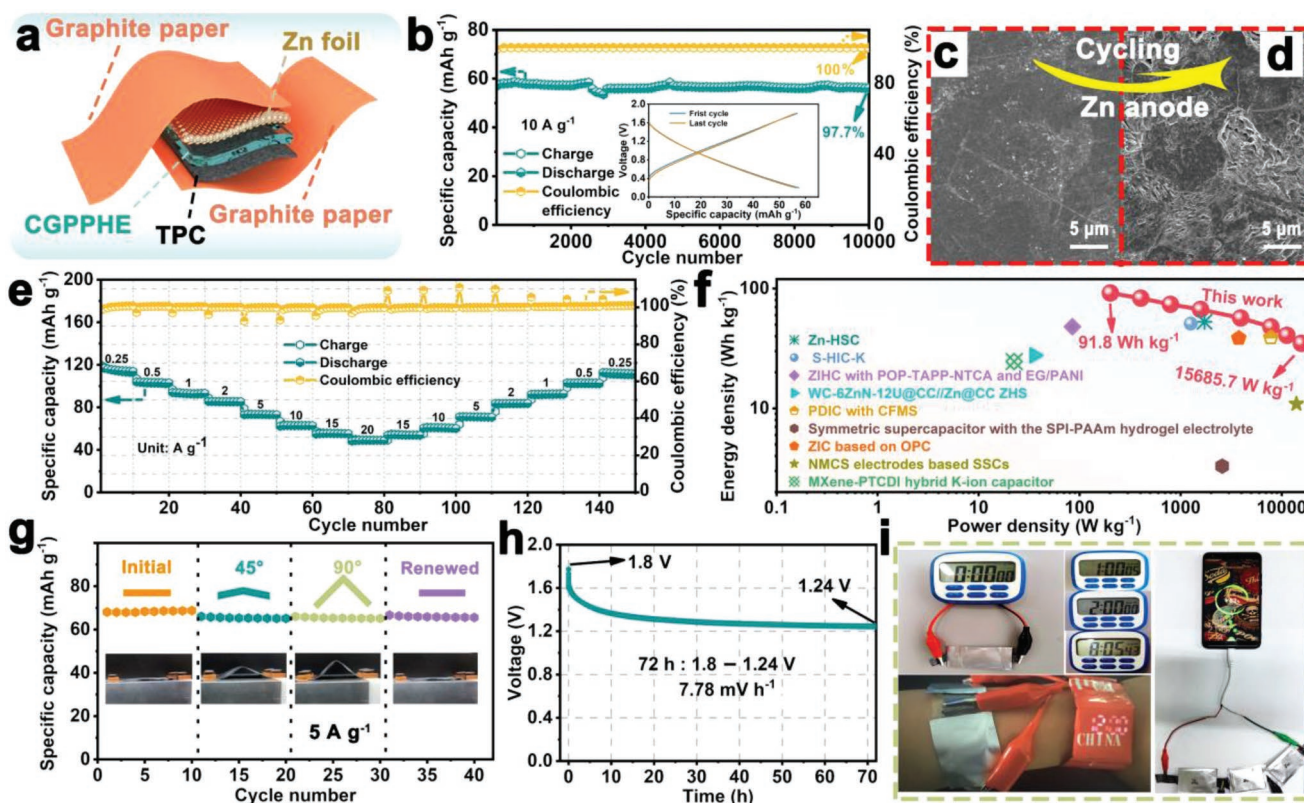


Figure 5. Electrochemical performance of flexible quasi-solid-state Zn|CGPPHE|TPC ZHC and its application. a) Structural diagram of the flexible quasi-solid-state Zn|CGPPHE|TPC device. b) Cyclic stability and CE at 10 A g^{-1} after 10 000 cycles (inset: the first and last GCD curves). SEM images of Zn anode c) before and d) after cycling. e) Rate performance and CE. f) Ragone plots of the fabricated ZHC compared with other reported devices. g) Specific capacities at 5 A g^{-1} at different bending states. h) Self-discharge curve. i) Digital photographs showing the application of the fabricated ZHC in the electronic timer, wearable electronic watch, and mobile phone.

parasitic corrosion and HER intensify the above-mentioned tip effect, leading to flagrant dendrite growth (Figure 4j). Yet, the tip effect in CGPPHE is efficiently repressed due to the multiple merits, including strong affinity, adjustment of Zn^{2+} diffusion mode, homogenization of Zn^{2+} flux and electric field, and reduction of adverse reactions (Figure 4k).

To evaluate the utility of CGPPHE, a flexible quasi-solid-state ZHC with the K_2FeO_4 template-guided porous carbon (TPC) as the cathode material was assembled (expressed as Zn|CGPPHE|TPC ZHC), as schematized in Figure 5a. Here, the TPC starting from coal tar pitch shows a porous shape with a long/short-range ordered structure and high surface area of $1992.1 \text{ cm}^2 \text{ g}^{-1}$, which is beneficial for promoting Zn^{2+} -storage properties (Figures S13 and S14, Supporting Information). Figure 5b indicates that the Zn|CGPPHE|TPC ZHC can work stably for 10 000 cycles at 10 A g^{-1} , with 97.7% capacity retention and $\approx 100\%$ CE, which undoubtedly justifies the long-term reversible cycle performance of the device. The embedded GCD curves with excellent overlap for the first and last cycles further reveal the outstanding cyclability of the constructed quasi-solid-state ZHC device (inset in Figure 5b). From Figure 5c,d, the Zn anode in the cycled Zn|CGPPHE|TPC device shows a relatively rough surface without obvious dendrites as compared to that before cycling, further confirming considerable stability of Zn anode in CGPPHE, similar to the result of the symmetric cell (Figure 3e).

Figure 5e presents the rate behavior of the Zn|CGPPHE|TPC ZHC. It offers a stable specific capacity of 113.7 mAh g^{-1} at 0.25 A g^{-1} , and obtains 103, 93.1, 85.3, 73, 62.7, 55.1, and 49 mAh g^{-1} at 0.5, 1, 2, 5, 10, 15, and 20 A g^{-1} , respectively, corresponding to a high retention rate of 43.1% in a wide range of $0.25\text{--}20 \text{ A g}^{-1}$. It is also found that the high capacity retention of 98.2% can be still achieved with the current density re-decreasing to 0.25 A g^{-1} . Moreover, the CE at each current density is stabilized at $\approx 100\%$. These results affirm that the as-built ZHC can tolerate large current rates and has high reversible storage ability benefiting from the multiple functions of CGPPHE. From Ragone plots in Figure 5f, the maximum energy density of the device reaches 91.8 Wh kg^{-1} at a power density of 201.7 W kg^{-1} , and the power density as high as $15\,685.7 \text{ W kg}^{-1}$ is delivered at an energy density of 34.9 Wh kg^{-1} . The energy density of the quasi-solid-state Zn|CGPPHE|TPC ZHC is higher than that of many related energy-storage devices like Zn-HSC (52.7 Wh kg^{-1} at 1725 W kg^{-1}),^[63] S-HIC-K (51 Wh kg^{-1} at 1260 W kg^{-1}),^[64] ZIHC with POP-TAPP-NTCA and EG/PANI (48 Wh kg^{-1} at 85 W kg^{-1}),^[65] WC-6ZnN-12U@CC//Zn@CC ZHS (27.7 Wh kg^{-1} at 35.7 W kg^{-1}),^[66] PDIC with CFMS (39 Wh kg^{-1} at 7800 W kg^{-1}),^[67] symmetric supercapacitor with the SPI-PAAm hydrogel electrolyte (21.4 Wh kg^{-1} at 130 W kg^{-1}),^[68] ZIC based on OPC (38.6 Wh kg^{-1} at 3760 W kg^{-1}),^[69] NMCS electrodes based SSCs (23.4 Wh kg^{-1} at 700.6 W kg^{-1}),^[70] and MXene-PTCDI

hybrid K-ion capacitor (24.6 Wh kg^{-1} at 22.5 W kg^{-1}).^[7] Additionally, this quasi-solid-state ZHC shows a negligible capacity change under different deformation states (initial, 45° , 90° , and renewed), indicating good flexibility of the device (Figure 5g).

The anti-self-discharge capability holds a pivotal role in high-efficiency energy storage. In order to gain this information, the Zn|CGPPHE|TPC ZHC was fully charged to 1.8 V and then rested for 72 h at room temperature to investigate the open circuit voltage change. The device maintains a high voltage of 1.24 V after 72 h with a low decline rate of 7.78 mV h^{-1} , reflecting the superior anti-self-discharge property (Figure 5h). Finally, the Zn|CGPPHE|TPC ZHC was applied in various portable electronics for evaluating its practicability. It shows that one ZHC can stably power the electronic timer over eight hours, two ZHCs in series can make the wearable electronic watch operate normally, and such three devices in series are able to charge the mobile phone, corroborating the potentiality of the flexible Zn|CGPPHE|TPC ZHC in the field of portable and wearable electronics (Figure 5i).

3. Conclusion

Summarily, we develop a CCS-enhanced CGPPHE that can greatly overcome Zn anode issues, thereby endowing the efficient storage ability of flexible ZHCs. The optimized multiple networks impart CGPPHE with the improved conductivity and mechanical properties compared with its counterparts (PHE and PPHE). It is also found that CGPPHE can reduce the desolvation penalty with low E_a (32.8 kJ mol^{-1}) and guide Zn^{2+} for 3D diffusion by introducing CCS with carboxyl groups assisted by PAM with amide groups, favoring fast kinetics and uniform Zn deposition. Besides, parasitic HER and corrosion are restrained by the reduced water activity contributed by hydrophilic groups in CGPPHE. These advantages enable the stable cycling over 350 h (1 mA cm^{-2} , 1 mAh cm^{-2}) and a high cumulative capacity of 1600 mAh cm^{-2} (20 mA cm^{-2} , 1 mAh cm^{-2}) for the Zn|CGPPHE|Zn cell as well as a high average CE of 98.2% for the Zn|CGPPHE|Cu cell. The assembled flexible quasi-solid-state Zn|CGPPHE|TPC device makes considerable energy and power densities (91.8 Wh kg^{-1} and $15\,685.7 \text{ W kg}^{-1}$), and works stably over 10 000 cycles with only 2.3% capacity loss. Findings will be of immediate benefit in designing and understanding multifunctional hydrogel electrolytes for more efficient ZHCs.

Supporting Information

Supporting Information is available from the Wiley Online Library or from the author.

Acknowledgements

C.L. and F.G. contributed equally to this work. The experiments involving human subjects have been performed with the full informed consent of the volunteer. This work was supported by National Natural Science Foundation of China (21965033 and U2003216), Shanghai Cooperation Organisation Project (2022E01020), Natural Science Foundation of Xinjiang Uygur Autonomous Region (2021D01C099), Opening Foundation of the State Key Laboratory of Fine Chemicals (KF2104), and

Opening Foundation of the Anhui Province Key Laboratory of Coal Clean Conversion and High Valued Utilization (CHV2102). The authors would like to thank Shiyanjia Lab for the measurement and analysis.

Open access funding enabled and organized by Projekt DEAL.

Conflict of Interest

The authors declare no conflict of interest.

Data Availability Statement

Research data are not shared.

Keywords

dendrite suppression, deposition behavior, polymer hydrogel electrolytes, zinc anodes, zinc-ion hybrid capacitors

Received: October 27, 2022

Published online:

- [1] J. Yin, W. Zhang, W. Wang, N. A. Alhebshi, N. Salah, H. N. Alshareef, *Adv. Energy Mater.* **2020**, *10*, 2001705.
- [2] L. Han, H. Huang, J. Li, X. Zhang, Z. Yang, M. Xu, L. Pan, *J. Mater. Chem. A* **2020**, *8*, 15042.
- [3] H. Tang, J. Yao, Y. Zhu, *Adv. Energy Mater.* **2021**, *11*, 2003994.
- [4] L. Han, H. Huang, X. Fu, J. Li, Z. Yang, X. Liu, L. Pan, M. Xu, *Chem. Eng. J.* **2020**, *392*, 123733.
- [5] Z. Zhao, J. Zhao, Z. Hu, J. Li, J. Li, Y. Zhang, C. Wang, G. Cui, *Energy Environ. Sci.* **2019**, *12*, 1938.
- [6] V. Yufit, F. Tariq, D. S. Eastwood, M. Biton, B. Wu, P. D. Lee, N. P. Brandon, *Joule* **2019**, *3*, 485.
- [7] X. Zhang, J. Li, D. Liu, M. Liu, T. Zhou, K. Qi, L. Shi, Y. Zhu, Y. Qian, *Energy Environ. Sci.* **2021**, *14*, 3120.
- [8] H. Peng, C. Liu, N. Wang, C. Wang, D. Wang, Y. Li, B. Chen, J. Yang, Y. Qian, *Energy Environ. Sci.* **2022**, *15*, 1682.
- [9] Y. Zhong, Z. Cheng, H. Zhang, J. Li, D. Liu, Y. Liao, J. Meng, Y. Shen, Y. Huang, *Nano Energy* **2022**, *98*, 107220.
- [10] L. Miao, R. Wang, S. Di, Z. Qian, L. Zhang, W. Xin, M. Liu, Z. Zhu, S. Chu, Y. Du, N. Zhang, *ACS Nano* **2022**, *16*, 9667.
- [11] H. Yu, Y. Chen, W. Wei, X. Ji, L. Chen, *ACS Nano* **2022**, *16*, 9736.
- [12] J. Gu, Y. Tao, H. Chen, Z. Cao, Y. Zhang, Z. Du, Y. Cui, S. Yang, *Adv. Energy Mater.* **2022**, *12*, 2200115.
- [13] D. Han, C. Cui, K. Zhang, Z. Wang, J. Gao, Y. Guo, Z. Zhang, S. Wu, L. Yin, Z. Weng, F. Kang, Q.-H. Yang, *Nat. Sustain.* **2022**, *5*, 205.
- [14] Z. Li, Y. An, S. Dong, C. Chen, L. Wu, Y. Sun, X. Zhang, *Energy Storage Mater.* **2022**, *31*, 252.
- [15] K. Wu, J. Huang, J. Yi, X. Liu, Y. Liu, Y. Wang, J. Zhang, Y. Xia, *Adv. Energy Mater.* **2020**, *10*, 1903977.
- [16] Y. Guo, J. Bae, Z. Fang, P. Li, F. Zhao, G. Yu, *Chem. Rev.* **2020**, *120*, 7642.
- [17] J.-L. Yang, J. Li, J.-W. Zhao, K. Liu, P. Yang, H. J. Fan, *Adv. Mater.* **2022**, *34*, 2202382.
- [18] K. Leng, G. Li, J. Guo, X. Zhang, A. Wang, X. Liu, J. Luo, *Adv. Funct. Mater.* **2020**, *30*, 2001317.
- [19] D. Xie, Z.-W. Wang, Z.-Y. Gu, W.-Y. Diao, F.-Y. Tao, C. Liu, H.-Z. Sun, X.-L. Wu, J.-W. Wang, J.-P. Zhang, *Adv. Funct. Mater.* **2022**, *32*, 2204066.
- [20] C. Li, X. Xie, S. Liang, J. Zhou, *Energy Environ. Mater.* **2020**, *3*, 146.

- [21] S. Jiao, J. Fu, M. Wu, T. Hua, H. Hu, *ACS Nano* **2022**, *16*, 1013.
- [22] Y. Yang, C. Liu, Z. Lv, H. Yang, Y. Zhang, M. Ye, L. Chen, J. Zhao, C. C. Li, *Adv. Mater.* **2021**, *33*, 2007388.
- [23] Q. Yang, L. Li, T. Hussain, D. Wang, L. Hui, Y. Guo, G. Liang, X. Li, Z. Chen, Z. Huang, Y. Li, Z. Zuo, J. Qiu, Y. Li, C. Zhi, *Angew. Chem., Int. Ed.* **2021**, *60*, 2.
- [24] H. Liu, J.-G. Wang, W. Hua, L. Ren, H. Sun, Z. Hou, Y. Huan, Y. Cao, C. Wei, F. Kang, *Energy Environ. Sci.* **2022**, *15*, 1872.
- [25] B. Zhang, L. Qin, Y. Fang, Y. Chai, X. Xie, B. Lu, S. Liang, J. Zhou, *Sci. Bull.* **2022**, *9*, 955.
- [26] Y. Hao, D. Feng, L. Hou, T. Li, Y. Jiao, P. Wu, *Adv. Sci.* **2022**, *9*, 2104832.
- [27] B. Wang, R. Zheng, W. Yang, X. Han, C. Hou, Q. Zhang, Y. Li, K. Li, H. Wang, *Adv. Funct. Mater.* **2022**, *23*, 2112693.
- [28] P. Lin, J. Cong, J. Li, M. Zhang, P. Lai, J. Zeng, Y. Yang, J. Zhao, *Energy Storage Mater.* **2022**, *49*, 172.
- [29] Q. Li, D. Wang, W. B. Yan, Y. Zhao, J. Fan, C. Zhi, *Angew. Chem., Int. Ed.* **2022**, *61*, 202202780.
- [30] H. Li, C. Han, Y. Huang, Y. Huang, M. Zhu, Z. Pei, Q. Xue, Z. Wang, Z. Liu, Z. Tang, Y. Wang, F. Kang, B. Li, C. Zhi, *Energy Environ. Sci.* **2018**, *11*, 941.
- [31] H. Yang, X. Ji, Y. Tan, Y. Liu, F. Ran, *J. Power Sources* **2019**, *441*, 227174.
- [32] G. Chen, J. Huang, J. Gu, S. Peng, X. Xiang, K. Chen, X. Yang, L. Guan, X. Jiang, L. Hou, *J. Mater. Chem. A* **2020**, *8*, 6776.
- [33] Y. Gutha, L. P. Janak, W. Zhang, Y. Zhang, X. Jiao, *Int. J. Biol. Macromol.* **2017**, *103*, 234.
- [34] H. Li, Z. Liu, G. Liang, Y. Huang, M. Zhu, Z. Pei, Q. Xue, Z. Tang, Y. Wang, B. Li, C. Zhi, *ACS Nano* **2018**, *12*, 3140.
- [35] S. Zeng, Z. Huang, H. Jiang, Y. Li, *ACS Appl. Mater. Interfaces* **2020**, *12*, 52038.
- [36] H. Yang, Y. Liu, L. Kong, L. Kang, F. Ran, *J. Power Sources* **2019**, *426*, 47.
- [37] X. Xu, X. Ouyang, L.-Y. Yang, *J. Mol. Liq.* **2021**, *322*, 114523.
- [38] M. Chen, J. Chen, W. Zhou, X. Han, Y. Yao, C.-P. Wong, *Adv. Mater.* **2021**, *33*, 2007559.
- [39] S. Huang, L. Hou, T. Li, Y. Jiao, P. Wu, *Adv. Mater.* **2022**, *34*, 2110140.
- [40] X. Zhao, X. Chen, H. Yuk, S. Lin, X. Liu, G. Parada, *Chem. Rev.* **2021**, *121*, 4309.
- [41] J. Xu, R. Jing, X. Ren, G. Gao, *J. Mater. Chem. A* **2020**, *8*, 9373.
- [42] Y. Zhang, T. Li, L. Miao, P. Kaur, S. Men, Q. Wang, X. Gong, Y. Fang, C. Zhai, S. Zhang, L. Zhang, L. Ye, *J. Mater. Chem. A* **2022**, *10*, 3970.
- [43] W. Zhang, B. Wu, S. Sun, P. Wu, *Nat. Commun.* **2021**, *12*, 4082.
- [44] Q. Fu, S. Hao, L. Meng, F. Xu, J. Yang, *ACS Nano* **2021**, *15*, 18469.
- [45] B. Wang, J. Li, C. Hou, Q. Zhang, Y. Li, H. Wang, *ACS Appl. Mater. Interfaces* **2020**, *12*, 46005.
- [46] Y. Shao, J. Zhao, W. Hu, Z. Xia, J. Luo, Y. Zhou, L. Zhang, X. Yang, N. Ma, D. Yang, Q. Shi, J. Sun, L. Zhang, J. Hui, Y. Shao, *Small* **2022**, *18*, 2107163.
- [47] W. Pan, Y. Wang, X. Zhao, Y. Zhao, X. Liu, J. Xuan, H. Wang, D. Y. C. Leung, *Adv. Funct. Mater.* **2021**, *31*, 2008783.
- [48] T. Zhang, Y. Tang, S. Guo, X. Cao, A. Pan, G. Fang, J. Zhou, S. Liang, *Energy Environ. Sci.* **2020**, *13*, 4625.
- [49] S. Li, J. Fu, G. Miao, S. Wang, W. Zhao, Z. Wu, Y. Zhang, X. Yang, *Adv. Mater.* **2021**, *33*, 2008424.
- [50] C. Fu, Y. Wang, C. Lu, S. Zhou, Q. He, Y. Hu, M. Feng, Y. Wan, J. Lin, Y. Zhang, A. Pan, *Energy Storage Mater.* **2022**, *51*, 588.
- [51] L. Ma, S. Chen, N. Li, Z. Liu, Z. Tang, J. A. Zapien, S. Chen, J. Fan, C. Zhi, *Adv. Mater.* **2020**, *32*, 1908121.
- [52] S. Di, X. Nie, G. Ma, W. Yuan, Y. Wang, Y. Liu, S. Shen, N. Zhang, *Energy Storage Mater.* **2021**, *43*, 375.
- [53] X. Liu, H. Euchner, M. Zarrabeitia, X. Gao, G. A. Elia, A. Groß, S. Passerini, *ACS Energy Lett.* **2020**, *5*, 2979.
- [54] Y. Zhang, X. Han, R. Liu, Z. Yang, S. Zhang, Y. Zhang, H. Wang, Y. Cao, A. Chen, J. Sun, *Small* **2022**, *18*, 2105978.
- [55] W. Zhou, M. Chen, Q. Tian, J. Chen, X. Xu, C.-P. Wong, *Energy Storage Mater.* **2022**, *44*, 57.
- [56] H. Jin, S. Dai, K. Xie, Y. Luo, Z. Zhu, L. Huang, L. Huang, J. Zhou, *Small* **2021**, *18*, 2106441.
- [57] C. Li, X. Xie, H. Liu, P. Wang, C. Deng, B. Lu, J. Zhou, S. Liang, *Natl. Sci. Rev.* **2022**, *9*, 177.
- [58] H. Lu, X. Zhang, M. Luo, K. Cao, Y. Lu, B. B. Xu, H. Pan, K. Tao, Y. Jiang, *Adv. Funct. Mater.* **2021**, *31*, 2103514.
- [59] C. Liu, X. Xie, B. Lu, J. Zhou, S. Liang, *ACS Energy Lett.* **2021**, *6*, 1015.
- [60] A. Bayaguud, X. Luo, Y. Fu, C. Zhu, *ACS Energy Lett.* **2020**, *5*, 3012.
- [61] Y. Geng, L. Pan, Z. Peng, Z. Sun, H. Lin, C. Mao, L. Wang, L. Dai, H. Liu, K. Pan, X. Wu, Q. Zhang, Z. He, *Energy Storage Mater.* **2022**, *51*, 733.
- [62] G. Liang, J. Zhu, B. Yan, Q. Li, A. Chen, Z. Chen, X. Wang, B. Xiong, J. Fan, J. Xu, C. Zhi, *Energy Environ. Sci.* **2022**, *15*, 1086.
- [63] H. Wang, M. Wang, Y. Tang, *Energy Storage Mater.* **2018**, *13*, 1.
- [64] Z. Xu, M. Wu, Z. Chen, C. Chen, J. Yang, T. Feng, E. Paek, D. Mitlin, *Adv. Sci.* **2019**, *19*, 1802272.
- [65] F. Cui, Z. Liu, D. Ma, L. Liu, T. Huang, P. Zhang, D. Tan, F. Wang, G. Jiang, Y. Wu, *Chem. Eng. J.* **2021**, *405*, 127038.
- [66] G. Lou, G. Pei, Y. Wu, Y. Lu, Y. Wu, X. Zhu, Y. Pang, Z. Shen, Q. Wu, S. Fu, H. Chen, *Chem. Eng. J.* **2021**, *413*, 127502.
- [67] Y. Feng, S. Chen, J. Wang, B. Lu, *J. Energy Chem.* **2020**, *43*, 129.
- [68] J. Nan, G. Zhang, T. Zhu, Z. Wang, L. Wang, H. Wang, F. Chu, C. Wang, C. Tang, *Adv. Sci.* **2020**, *22*, 2000587.
- [69] Y. Zheng, W. Zhao, D. Jia, Y. Liu, L. Cui, D. Wei, R. Zheng, J. Liu, *Chem. Eng. J.* **2020**, *387*, 124161.
- [70] Y. Qiu, M. Hou, J. Gao, H. Zhai, H. Liu, M. Jin, X. Liu, L. Lai, *Small* **2019**, *6*, 1903836.
- [71] G. Liang, X. Li, Y. Wang, S. Yang, Z. Huang, Q. Yang, D. Wang, B. Dong, M. Zhu, C. Zhi, *Nano Res. Energy* **2022**, *1*, 9120002.